Chemical Engineering Journal 535 (2026) 175634

Contents lists available at ScienceDirect

Chemical Engineering Journal

journal homepage: www.elsevier.com/locate/cej

Bridging accelerated cell-level degradation to module-relevant failure mechanisms in TOPCon solar cells and modules

Xinyuan Wu [a,*], Wei Wu [b], Weiguang Yang [b], Yan Zhang [b], Jiexi Fu [a], Xutao Wang [a], Jing Yuan [b], Jianjun Nie [b], Zhencong Qiao [b], Chao An [b], Feng Li [b], Lin Lv [b], Baochen Liao [c], Bram Hoex [a,*]

[a] School of Photovoltaic and Renewable Energy Engineering, University of New South Wales, Sydney, 2052, Australia
[b] Jolywood (Taizhou) Solar Technology Co., Ltd., Taizhou, Jiangsu, 225500, China
[c] School of Information Science and Technology, Nantong University, Jiangsu, 226019, China

ARTICLE INFO

Keywords:
TOPCon
Solar module
Reliability
Damp-heat
Degradation
Laser-assisted firing
LECO
Metallisation

ABSTRACT

Tunnel oxide passivated contact (TOPCon) solar cells are the dominant industrial photovoltaic (PV) technology; however, their long-term reliability under damp-heat conditions remains a critical bottleneck, particularly for cost-driven, low bill-of-materials (BOM) module designs. Conventional solution-based accelerated ageing methods, such as acetic acid (CH_3COOH) immersion or alkaline soaking, impose chemically unrealistic and non-selective stress conditions and often fail to reproduce module-level degradation trends, thereby limiting their predictive value. In this work, we establish a chemically relevant cell-level accelerated ageing method based on nitrate-induced, pH-controlled contamination to bridge short-term cell-level testing with long-term module degradation behaviour. By combining nitrate anions with different cations, the solution acidity is systematically tuned and selectively applied to the front surface of tunnel oxide passivated contact (TOPCon) solar cells, enabling targeted evaluation of front-side metallisation stability under ethylene vinyl acetate (EVA)-related mildly acidic environments. Two industrially relevant front-side TOPCon contacts, conventional Ag/Al paste and low-Al Ag paste [enabled by laser-assisted firing (LAF)], are comparatively investigated. The analysis indicates a pronounced pH-dependent degradation behaviour, whereby increasingly acidic nitrate environments lead to progressively more severe contact corrosion, resulting in increased series resistance and corresponding losses in fill factor and power conversion efficiency. Under weakly acidic nitrate conditions representative of EVA-encapsulated modules, the resulting cell-level degradation fingerprints show good qualitative consistency with module-level damp-heat behaviour. Overall, this work demonstrates that chemically selective, pH-controlled nitrate ageing provides a physically meaningful and predictive accelerated testing framework for TOPCon solar cells, enabling reliable discrimination of metallisation concepts and offering a robust pathway to assess and improve long-term device stability for PV modules.

1. Introduction

Tunnel oxide passivated contact (TOPCon) solar cells have emerged as the leading industrial photovoltaic technologies, owing to their high power conversion efficiency (PCE), excellent surface passivation, and strong compatibility with large-scale manufacturing [1–3]. According to the latest International Technology Roadmap for Photovoltaics (ITRPV), TOPCon technology is expected to continue dominating the global PV market throughout this decade [2]. However, in recent years, the rapid expansion of TOPCon manufacturing capacity has led to market over-capacity, driving product prices to historically low levels and significantly compressing profit margins. As a result, major PV manufacturers are now under increasing pressure to reduce the cost of TOPCon modules while maintaining high conversion efficiency, in order to enhance the market competitiveness of their products.

Low-cost bills of materials (BOMs) are widely regarded as a key pathway toward cost-effective module manufacturing [2,4,5]. However, their adoption may introduce additional reliability risks for emerging high-efficiency technologies such as TOPCon. Compared with conventional PERC modules, TOPCon devices have been reported to be more sensitive to several environmental and electrical stress conditions, including potential-induced degradation (PID) [6], damp-heat-induced

* Corresponding author.
E-mail addresses: xinyuan.wu@unsw.edu.au (X. Wu), b.hoex@unsw.edu.au (B. Hoex).

https://doi.org/10.1016/j.cej.2026.175634
Received 8 February 2026; Received in revised form 22 March 2026; Accepted 26 March 2026
Available online 27 March 2026

corrosion [7,8], and ultraviolet-induced degradation (UVID) [9,10]. Among these stressors, corrosion and related failure modes under damp-heat testing or humid operating conditions have emerged as a particularly critical concern [11].

For the early generations of TOPCon solar cells and modules, front-side metallisation using conventional silver/aluminium (Ag/Al) paste combined with a standard firing process has been identified as a dominant degradation pathway, leading to increased series resistance (R_s) and substantial fill factor (FF) losses [7,12–14]. The relatively high Al content in these Ag pastes is beneficial for forming low-resistance contacts with boron-doped emitters, but it can also induce Al spiking into the silicon (Si), thereby increasing surface recombination. Moreover, Al-containing contacts are prone to oxidation under damp-heat conditions, which further accelerates contact degradation and exacerbates series resistance growth and FF loss at both the solar cell and module levels [12,15]. Consistent with this mechanism, pronounced metallisation-related degradation fingerprints have been widely observed in TOPCon modules after damp-heat exposure [8,16,17].

These issues have been partially mitigated through the introduction of low-Al Ag pastes combined with laser-assisted firing (LAF), often referred to as laser-enhanced contact optimisation (LECO). Previous studies, including our own work, have demonstrated that this metallisation strategy significantly reduces module-level degradation under damp-heat treatment [7,15]. Reducing the Al content not only improves solar cell and module power conversion efficiency, particularly through enhanced open-circuit voltage (V_{oc}), but also enhances the stability of TOPCon devices by suppressing contact corrosion [15,18,19]. However, in glass–backsheet (G–B) TOPCon module configurations, which are increasingly adopted to reduce module weight and cost, the higher moisture permeability of the backsheet allows greater ingress of water vapour into the modules [20]. In addition, ageing of encapsulant materials can lead to the release of organic acids, resulting in a more acidic internal module environment [20,21]. Under these conditions, even LAF-processed TOPCon devices remain vulnerable, and further optimisation is required to ensure long-term reliability and compliance with module warranty requirements.

The standard damp heat testing protocol defined in IEC 61215 typically requires thousands of hours to evaluate a given bill of materials in combination with a specific solar cell technology. To accelerate the assessment of TOPCon stability, solution-based ageing methods, most notably immersion in acetic acid (CH_3COOH), which can be generated via hydrolysis of ethylene vinyl acetate (EVA), have been widely adopted to simulate the potential chemical environment experienced by solar cells inside modules [14,22–25]. While these approaches have provided valuable mechanistic insights, they suffer from several inherent limitations. Bulk soaking exposes both sides of the solar cell simultaneously, making selective evaluation of degradation on each side difficult. In addition, the chemical severity of concentrated acids or bases often exceeds that of mildly acidic environments that develop inside encapsulated modules during long-term damp heat exposure. As a result, conventional soaking tests do not reliably reproduce module-level degradation trends.

To address these shortcomings, several studies have introduced additional contaminants, such as sodium chloride (NaCl) and sodium bicarbonate ($NaHCO_3$), by spraying solutions onto solar cell surfaces followed by damp heat exposure [12,15,26–30]. However, recent work by Park et al. has shown that the internal pH of EVA encapsulated modules is close to about 5, creating only a mildly acidic environment for the embedded solar cells [31]. Consequently, commonly used neutral or alkaline salts cannot accurately represent the chemical conditions present inside real modules. In this context, nitrate species are more relevant, as they are ubiquitous in both the environment and module glass [32–34]. Nitrate is the conjugate base of nitric acid (HNO_3), a strong acid. Nitrate salts formed from a strong acid and a strong base, such as sodium nitrate ($NaNO_3$) or potassium nitrate (KNO_3), typically yield neutral solutions, whereas nitrates associated with weaker bases or specific metal cations [e.g., aluminium nitrate, $Al(NO_3)_3$, zinc nitrate, $Zn(NO_3)_2$; ammonium nitrate, NH_4NO_3] could produce acidic solutions [35,36]. As a result, the solution pH can be systematically adjusted by selecting nitrate salts with different cations. Although nitrate ions (NO_3^-) are stable in neutral, non-reducing environments, they become more reactive under acidic conditions due to protonation and can undergo reduction under certain conditions, which may in turn accelerate metal oxidation [35,36]. Compared with other inorganic anions, nitrate is chemically less complex, does not readily form insoluble precipitates with Ag under mildly acidic conditions in the absence of halide species. Nitrate ions are widely distributed in natural environments, including atmospheric deposition, soil and agricultural runoff, and aqueous systems, and may also be associated with nitrate-containing additives or chemical treatments used in certain glass processing or strengthening steps [32–34,37,38]. This makes nitrate-based systems particularly suitable for constructing chemically relevant accelerated ageing conditions.

In this work, we first evaluate the effects of CH_3COOH and alkaline soaking on Ag/Al and Low-Al Ag TOPCon solar cells and critically assess their limitations in the TOPCon solar cells by comparison with corresponding module-level degradation behaviour. Building on these insights, we develop a nitrate-based single-side ageing approach in which acidity is tuned by combining nitrate anions with different cations commonly present in photovoltaic materials. Controlled-pH contaminants are selectively applied to the front surface of TOPCon solar cells, followed by damp-heat exposure, enabling targeted evaluation of front-side metallisation stability under chemically realistic stress conditions. Two industrially relevant metallisation methods, conventional Ag/Al paste and low-Al Ag paste combined with LAF, are systematically investigated. Through comprehensive electrical characterization, microstructural analysis, and contact resistivity measurements, together with direct comparison with module-level damp-heat degradation fingerprints, we demonstrate that nitrate-based cell-level ageing provides a potential framework for accelerated reliability testing of TOPCon devices. More importantly, this work offers new insights into the design of chemically realistic accelerated ageing protocols for photovoltaic modules.

2. Experimental details

All TOPCon solar cells were fabricated on G10 n-type Czochralski (Cz) silicon wafers with dimensions of 182 mm × 183.75 mm. Two solar cell variants were prepared, differing primarily in their front-contact metallization schemes. The baseline solar cells employed a conventional commercial Ag/Al paste with an Al content of 3–5 at.% processed by a standard firing technique. These solar cells are hereafter referred to as Ag/Al. In contrast, the second group utilized Jolywood Special Injected Metallization (JSIM), which integrates a customized low-Al Ag paste with Al $<$ 0.2 at.% and a laser-assisted firing process under reverse-bias conditions to form the front contacts. These solar cells are referred to as Ag/LAF.

Prior to module fabrication, all solar cells were half-cut using a low-damage laser process, yielding modules composed of 144 half-cells. As illustrated in Fig. 1, the G-B module architecture employed EVA as the encapsulant on both the front and rear sides. A UV-blocking EVA layer with an areal weight of 420 g/m^2 was applied to the front side, while 420 g/m^2 of UV-transparent EVA was used on the rear side. The modules were completed with a transparent backsheet featuring a white grid pattern. Module level damp-heat testing (DH85) was conducted at 85 °C and 85% relative humidity in accordance with IEC TS 62782:2016, with output measurements performed using a Gsolar Power GIV 200DS2616 flash tester [39]. The relative change ($\%_{rel}$) was calculated as (X_aged − X_initial) / X_initial × 100%, where negative values indicate parameter degradation after ageing. Following DH85 exposure, current-voltage (I—V) parameters and electroluminescence (EL) images were re-measured using the same system to identify degradation fingerprints.

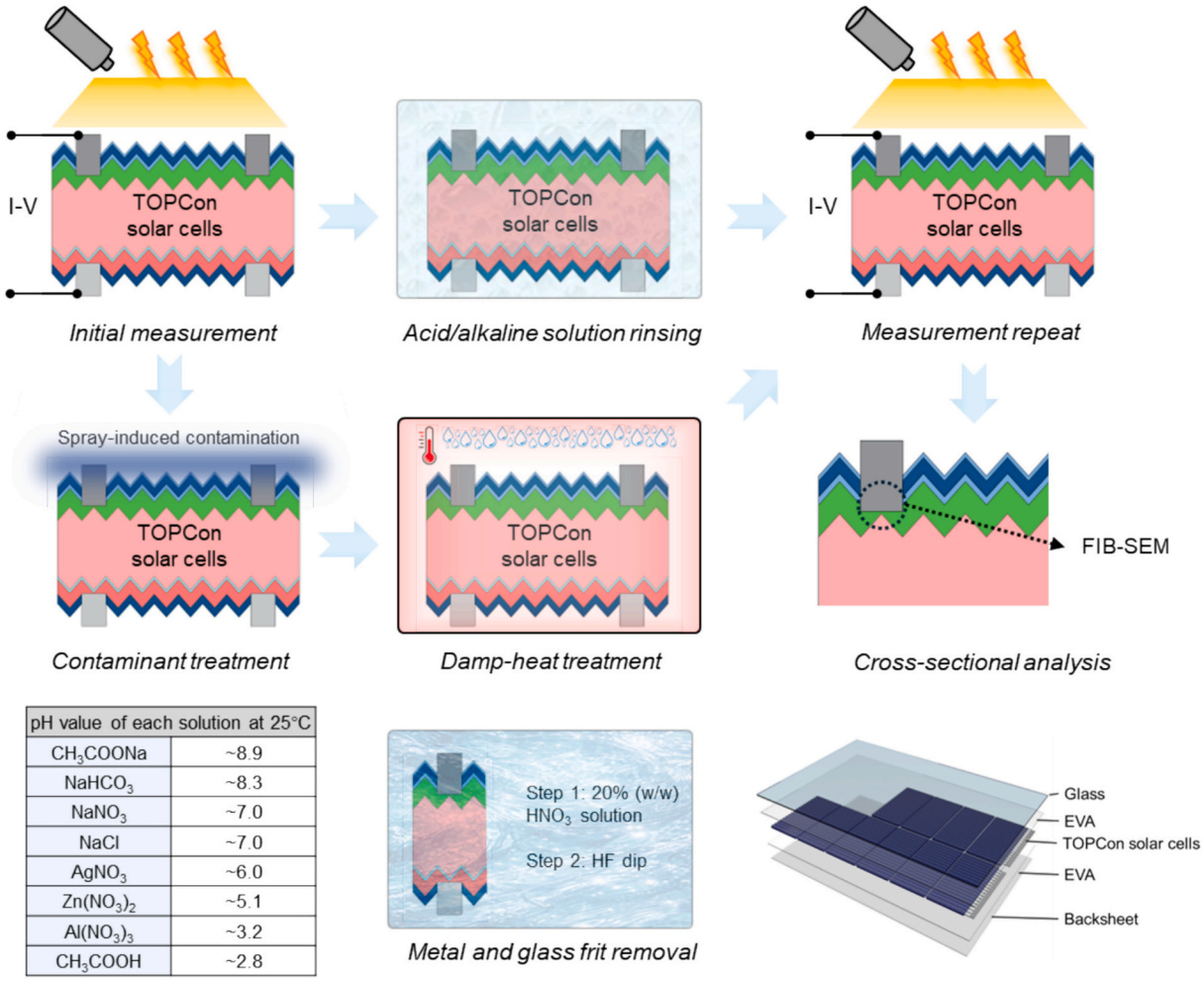

pH value of each solution at 25°C	
CH_3COONa	~8.9
$NaHCO_3$	~8.3
$NaNO_3$	~7.0
NaCl	~7.0
$AgNO_3$	~6.0
$Zn(NO_3)_2$	~5.1
$Al(NO_3)_3$	~3.2
CH_3COOH	~2.8

Fig. 1. The figure illustrates the experimental preparation and treatment procedures, including solution exposure under controlled pH conditions, surface contamination, post-treatment processing, and subsequent characterization of TOPCon solar cells, as well as the schematic of the TOPCon modules evaluated in this work.

Cell-level testing was performed using two accelerated stress methods. In the first protocol, solar cells were immersed in 250 mL of either 0.1 mol/L (0.57 vol%) CH_3COOH solution or 0.1 mol/L sodium acetate (CH_3COONa) solution and subsequently subjected to thermal treatment at 85 °C for 5 h. In the second method, we used the method we applied in our previous research and selected salt solutions were uniformly sprayed onto the front surface of the solar cells, with approximately 0.4 g of a 0.155 mol/L solution applied to each sample [12,15,29]. The solution concentration was normalised with respect to the anion species. After air drying, the solar cells were also exposed to DH85 without any encapsulant in an ASLi environmental chamber. It should be noted that the pH values of all solutions were calculated at 25 °C and are summarized in Fig. 1. Temperature-dependent variations in absolute acidity may occur during ageing at 85 °C, while the relative acidity trend among the tested salt solutions is expected to remain consistent. In spray-based tests, after solvent evaporation, the effective local pH at the cell surface is expected to deviate from the initial bulk solution pH. Nevertheless, the relative pH trend across the different salt solutions remains consistent, enabling meaningful comparison of their chemical aggressiveness. For each test condition, at least three samples were evaluated to ensure reproducibility and to minimize sporadic effects, and the average relative I—V parameters were used for comparative analysis comparison.

Electrical performance was measured before and after each test, and relative changes in I—V parameters were evaluated using a LOANA solar cell analysis system from pv-tools. A BT Imaging R3 system equipped with a high V_{oc} lens was used to acquire photoluminescence (PL) and series resistance (R_s) images. All luminescence measurements were performed on the front side of the TOPCon cells. Image processing was carried out using LumiTools [40]. The exposure time was adjusted to avoid signal saturation, and a 0–20 $\Omega \cdot cm^2$ range was used for R_s mapping [40]. To measure contact resistivity, non-busbar regions of the solar cells were selected and laser-scribed into 6 mm wide stripes using a FOBA M1000 system. The contact resistivities (ρ_c) of the front sides were determined by the transfer length method (TLM) using a pv-tools TLM-SCAN+.

For detailed contact analysis, untreated TOPCon solar cells were diced into 1 cm × 1 cm tokens. The samples were first rinsed in 20 wt% HNO_3 at room temperature for 2 h to completely remove the Ag fingers, followed by an HF dip to eliminate residual glass frit. Token samples were collected after each processing step, and scanning electron microscopy (SEM) was used to obtain plan-view images of the fingers in the as-received, post-HNO_3, and post-HF conditions. Top-view SEM images were acquired using a FEI Nova NanoSEM 450 field-emission SEM at an accelerating voltage of 15 kV.

Cross-sectional imaging of the metal contacts was performed using a Zeiss 550 Crossbeam cryo-focused ion-beam scanning electron microscope (cryo-FIB-SEM). The SEM operated at a probe current of 4 nA and an electron high-tension (EHT) voltage of 15 kV. During FIB milling, the stage was tilted to 54° relative to the ion beam and 36° relative to the

sample surface for imaging, and the SEM images and scales were adjusted accordingly. For elemental analysis, the FIB probe was operated at 30 kV and 50 pA in standard mode. Energy-dispersive spectroscopy (EDS) was performed under identical SEM conditions using an Oxford Instruments Ultim® Max detector. Data processing with AZtec software provided quantitative information on elemental distribution and ratios [41].

3. Results

3.1. Limitations of solution-based accelerated testing for evaluating TOPCon cell reliability

Following previous studies that evaluated TOPCon solar cells via immersion in CH_3COOH solutions, the chemical stability of the devices was investigated using a similar methodology [13,14,22,23]. To better simulate damp-heat stress conditions, the CH_3COOH solution was heated to 85 °C, and the solar cells were immersed in 0.1 mol/L CH_3COOH for 5 h. The resulting changes in electrical performance are summarized in Fig. 2a. For comparison, solar cells were also subjected to the same thermal treatment in a CH3COONa solution at the same ionic concentration.

Prior to ageing, the Ag/Al TOPCon solar cells exhibited an average measured PCE of 24.4%, a short-circuit current density (J_{sc}) of 41.0 mA/cm^2, an V_{oc} of 724.5 mV, and a FF of 82.3%. The Ag/LAF solar cells showed superior initial performance, with a PCE of 25.1%, J_{sc} of 41.2 mA/cm^2, V_{oc} of 733.5 mV, and FF of 83.2%.

After CH_3COOH treatment, both cell types exhibited pronounced degradation, with markedly different responses. The Ag/Al solar cells experienced a relative PCE loss of 21.1%$_{rel}$, primarily driven by a reduction in FF of 13.9%$_{rel}$, while J_{sc} and V_{oc} decreased by 8.5%$_{rel}$ and 0.1%$_{rel}$, respectively. In contrast, the Ag/LAF solar cells suffered severe performance deterioration, with a PCE reduction of 85.4%$_{rel}$. This degradation was dominated by substantial decreases in FF (69.1%$_{rel}$) and J_{sc} (52.0%$_{rel}$), whereas V_{oc} showed only a minor change (1.1%$_{rel}$). The pronounced reduction in J_{sc} is likely associated with the severe FF loss and extensive contact failure, leading to inefficient current extraction, consistent with our previous observations [12].

A similar trend was observed after CH_3COONa treatment, although the overall degradation was significantly less severe than that induced by CH_3COOH. The Ag/Al solar cells exhibited only a minor relative PCE reduction of 2.0%, accompanied by small decreases in J_{sc} (1.0%$_{rel}$) and FF (0.8%$_{rel}$), while V_{oc} remained essentially unchanged. The Ag/LAF solar cells again showed greater sensitivity, with a moderate relative PCE loss of 7.4%, mainly attributable to reductions in FF (6.2%$_{rel}$) and J_{sc} (1.1%$_{rel}$), with negligible variation in V_{oc}.

Furthermore, examination of the front-side contacts after CH_3COOH treatment, as shown in Fig. 2b, reveals a pronounced reduction in the adhesion strength of the Ag/LAF fingers. In contrast to the Ag/Al contacts, which largely remained mechanically intact under identical conditions, a fraction of the Ag/LAF fingers detached during the sample taken from the solutions, while the remaining fingers could be readily delaminated under minor external mechanical stress. Notably, under the same testing conditions, contact degradation on the rear side was relatively minor, as supported by the TLM results presented in Fig. S1. And the dominant failure mode was clearly associated with the front-side contacts.

To clarify the differences between the two metallization approaches, top-view SEM images were examined. As shown in Fig. 2c, the as-fabricated fingers have similar widths, although the Ag/LAF fingers

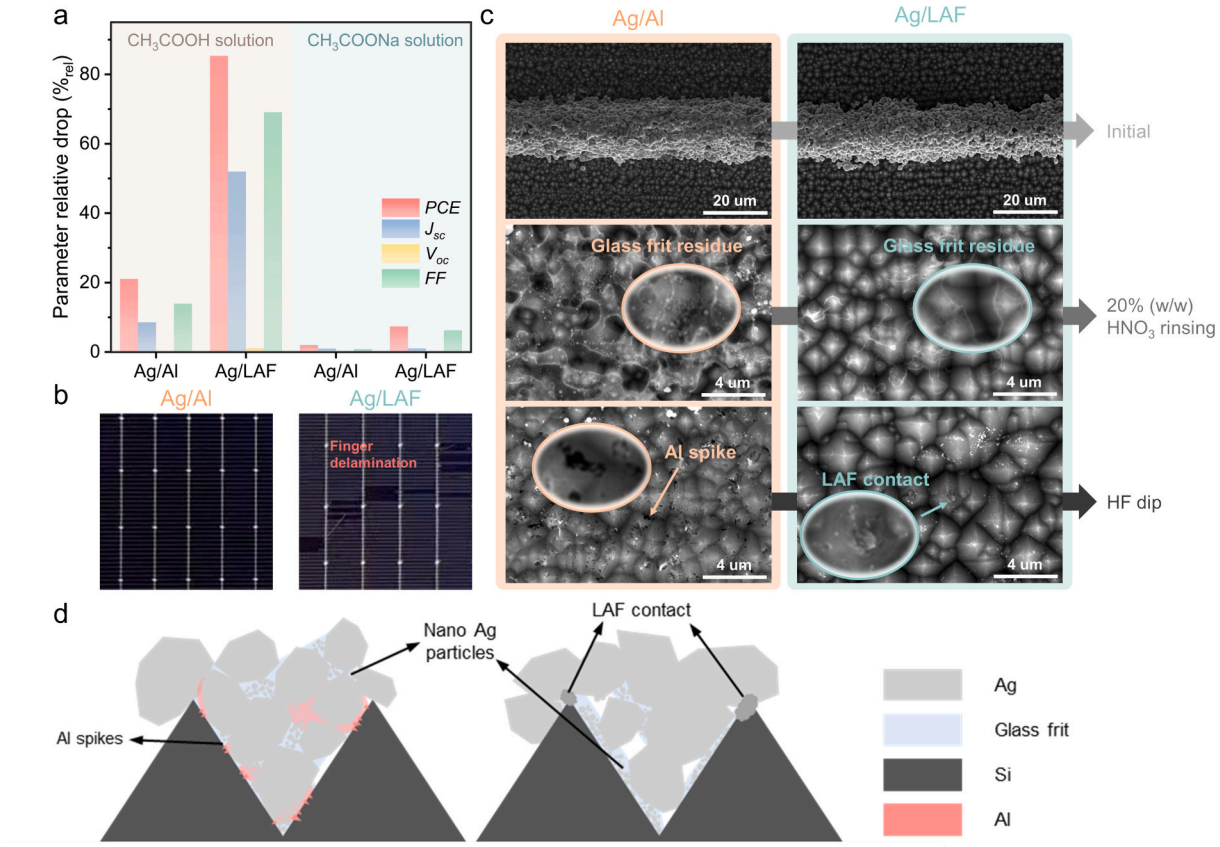

Fig. 2. (a) Relative I—V parameter variations of TOPCon solar cells after immersion in CH_3COOH and CH_3COONa solutions, (b) Top-view optical images of the front-side metal contact region after accelerated ageing in CH_3COOH solution, (c) top-view contact images of fresh, Ag-removed (after 20 wt% HNO_3 rinsing), and glass-frit-removed (after HF dip) samples, and (d) schematic illustrations of the Ag/Al and Ag/LAF contact structures.

are slightly thinner than the Ag/Al fingers. After removal of the bulk Ag finger material, the Ag/Al samples show a much larger amount of remaining glass-frit, while only limited residues are observed on the Ag/LAF samples. After complete removal of the glass frit layer, a high density of pits can be clearly seen on the pyramidal Si surface beneath the Ag/Al contacts. These pits are attributed to the removal of Al spikes formed during the Ag/Al firing process. As presented in Fig. 2d, although such Al spikes are known to reduce the contact resistivity of TOPCon front-side contacts, they can also increase contact-related recombination [42–46]. In contrast, the Ag/LAF contacts largely preserve the original Si pyramid surface. Localized Ag—Si alloy formation is mainly observed at the top of selected pyramids, which is sufficient to enable current extraction from the emitter [18]. As reported by Fan et al., standard Ag/Al pastes generally contain a higher fraction of glass frit compared with low-Al Ag pastes [47]. For these two types of TOPCon contacts, electrical conduction across the contact interface is also supported by Ag nanoparticles (AgNPs) embedded in the glass frit, which provide tunnelling paths through the interfacial layer [48].

During acid or alkaline soaking, the solution can readily penetrate along the finger and silicon interface and initiate chemical reactions at the metal semiconductor contact. This effect is particularly pronounced for the Ag/LAF TOPCon solar cells. Owing to the substantially lower glass frit content, the contact interface in Ag/LAF solar cells is governed by a thin glass frit layer that is rich in PbO. This PbO-rich glass frit is chemically unstable in CH_3COOH and undergoes preferential dissolution. As a result, the interfacial bonding between the silver finger and the textured silicon surface is progressively weakened, leading to a pronounced reduction in contact adhesion and ultimately triggering finger delamination [14,22,24].

In contrast, although Ag/Al contacts also undergo chemical interaction with the solution, their contact formation is primarily governed by Al spike penetration into the silicon surface. The higher glass frit content also provides a stronger mechanical bond between the silver and the textured silicon pyramids. Under the relatively mild CH_3COOH conditions employed in this study, corrosion of the glass frit in Ag/Al contacts appears to be comparatively limited. The resulting degradation behaviour may be influenced by a combination of factors, including interfacial transport processes within the glass phase and the intrinsic reactivity of Al-containing metallic constituents. At present, these considerations are proposed as plausible interpretations rather than definitive mechanisms, as direct experimental investigation of the governing corrosion kinetics and glass-phase reactions was beyond the scope of this work. Consequently, the electrically active Al—Si contact structure is largely preserved under the applied ageing conditions, leading to a comparatively smaller loss of contact integrity than that observed for Ag/LAF contacts. Based on our previous evaluations of TOPCon modules under DH85 conditions, modules fabricated using Ag/LAF TOPCon solar cells exhibited less degradation than those based on Ag/Al solar cells [7,15]. These results indicate that accelerated testing of isolated TOPCon solar cells by CH_3COOH soaking or alkaline solution exposure has inherent limitations in predicting module-level reliability. In particular, such solution-based treatments do not adequately reproduce the degradation trends observed at the module scale. Moreover, when CH_3COOH is used to accelerate cell degradation, selective single-sided evaluation is difficult to achieve, as both sides of the cell are simultaneously exposed to the solution. These factors restrict the applicability of conventional solution-based accelerated tests for simulating module-level degradation in TOPCon solar cells. Therefore, new cell-level accelerated testing approaches are required to more accurately represent degradation mechanisms relevant to module operation.

3.2. Single-side salt treatment for probing pH-dependent front-contact degradation

Considering the limitations of conventional soaking tests, a single-sided treatment method was developed for TOPCon solar cells by spraying selected solutions onto the front surface, with a primary focus on evaluating front-side contact degradation. Fig. 3a–d shows the relative changes in I—V parameters as a function of the salt solution pH, and the corresponding numerical data are summarized in Table S1.

Among the tested solutions, $Al(NO_3)_3$, which has a pH value closest to that of CH_3COOH, induced the most pronounced degradation. The relative PCE losses reached approximately 12.8% for Ag/Al solar cells and 76.1% for Ag/LAF solar cells. This degradation was mainly driven by a strong reduction in the FF for both contact types. The relative increase in series resistance was around 2000% for the $Al(NO_3)_3$-treated Ag/Al solar cells and about 8200% for the Ag/LAF solar cells, which is likely the primary cause of the FF drop. In addition, the Ag/LAF solar cells treated with $Al(NO_3)_3$ exhibited a J_{sc} decrease similar to that observed in the previous acetic-acid soaking tests. Together with the subsequent finger adhesion results shown in Fig. S2, this suggests comparable degradation behaviour associated with deteriorated contact integrity and impaired current extraction, although the underlying degradation mechanisms may involve multiple coupled processes.

For the $Zn(NO_3)_2$ groups, the relative PCE reductions were about 3.4% for Ag/Al solar cells and 2.8% for Ag/LAF solar cells. In these samples, the dominant contribution to performance loss again originated from FF degradation, while no evident decreases in J_{sc} or V_{oc} were observed for either contact type.

When treated with $AgNO_3$, the solar cells showed more degradation than in the $Zn(NO_3)_2$ groups, with relative PCE losses of approximately 4.5% for Ag/Al solar cells and about 3.0% for Ag/LAF solar cells. In contrast to the $Zn(NO_3)_2$ case, the FF reduction in the $AgNO_3$-treated samples was relatively smaller. However, a more pronounced J_{sc} decrease was observed for both cell types. This behaviour is likely related to the limited chemical stability of $AgNO_3$ under damp-heat conditions. $AgNO_3$ can decompose and form Ag or Ag_2O, which may precipitate as non-transparent particles on the front surface of the TOPCon solar cells [49,50]. Such surface contamination can partially block incident light and hinder current extraction, thereby leading to an additional loss in J_{sc}.

For the $NaNO_3$ groups, a slight PCE degradation of about 3.3% relative was observed for Ag/Al solar cells, mainly associated with an increase in R_s of around 370%. In contrast, no evident degradation was found for the Ag/LAF solar cells, with only a 0.28% relative PCE loss, a 0.24% relative FF drop, and a 10.5% increase in R_s, which can be regarded as negligible. This suggests that $NaNO_3$-induced near-neutral ageing conditions may promote contact degradation in Ag/Al cells by enhancing electrolyte conductivity and enabling electrochemical corrosion at the metal–silicon interface, potentially contributing to Al dissolution within the contact structure [12].

In the case of $NaHCO_3$, the PCE reduction of Ag/Al solar cells at 1.3% relative was slightly smaller than that of Ag/LAF solar cells at 1.5% relative after 24 h. In our previous work, $NaHCO_3$ and CH_3COONa were shown to exhibit similar chemical interactions with silicon solar cells, with their impact primarily arising from their alkaline nature and the resulting corrosion driven by hydroxide (OH^-) ions generated through hydrolysis. Notably, $NaHCO_3$ was found to require approximately 100 h to induce evident degradation; therefore, the minor degradation observed in the present study is reasonable [12,28]. Moreover, the alkaline environment induced more pronounced degradation in Ag/LAF TOPCon solar cells, which is consistent with our earlier observations from soaking tests.

We further examined the ρ_c to identify the origin of the observed increase in R_s. The initial ρ_c values of the Ag/Al contacts were in the range of 0.4–0.6 $m\Omega \cdot cm^2$, whereas the Ag/LAF contacts exhibited higher values of 1.9–2.5 $m\Omega \cdot cm^2$. The relatively higher ρ_c of the Ag/LAF contacts has also been reported in previous studies and is primarily attributed to a distinct mechanism of contact formation. In the present work, the lower front-contact resistivity of the Ag/Al solar cells is likely due to selective emitter regions that locally increase the doping concentration, thereby reducing the contact resistivity compared with lightly doped

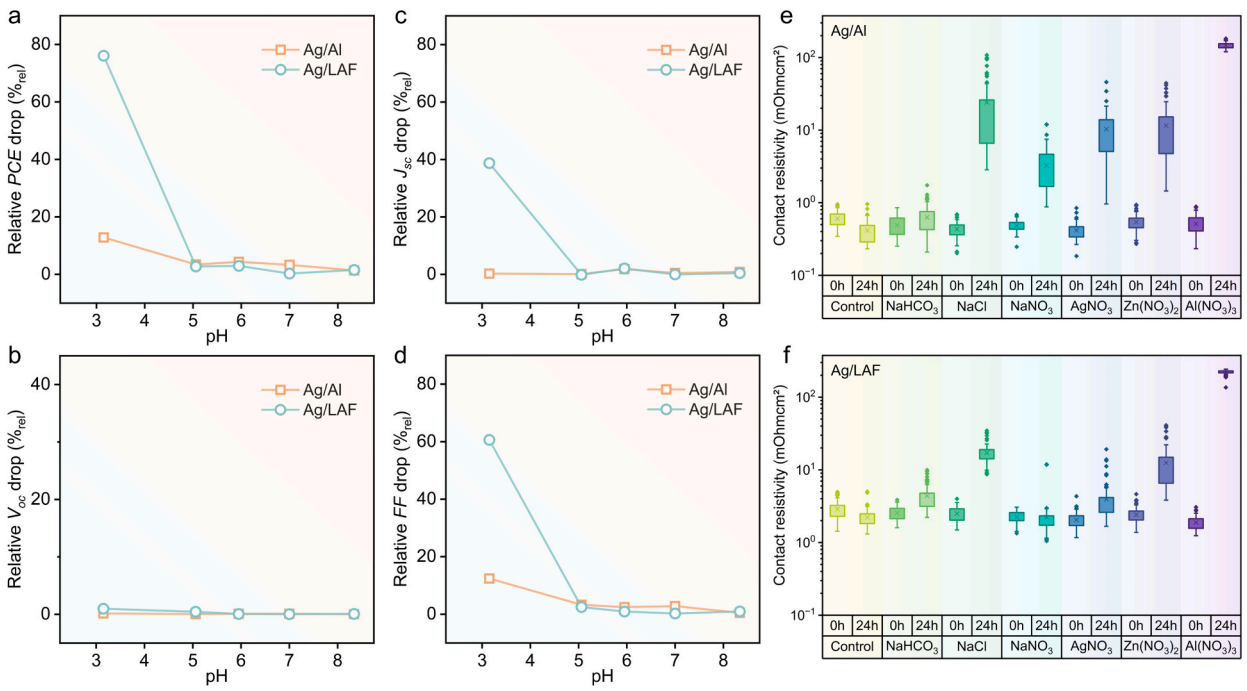

Fig. 3. Relative changes in I—V parameters of TOPCon solar cells after 24 h of DH85 exposure following treatment with 0.155 mol/L solutions of different pH values: $NaHCO_3$ (pH ≈ 8.3), $NaNO_3$ (pH ≈ 7.0), $AgNO_3$ (pH ≈ 6.0), $Zn(NO_3)_2$ (pH ≈ 5.1), and $Al(NO_3)_3$ (pH ≈ 3.2)(a) PCE, (b) V_{oc}, (c) J_{sc}, and (d) FF, together with contact resistivity before and after accelerated treatment for (e) Ag/Al and (f) Ag/LAF contacts in the presence of additional NaCl (pH ≈ 7.0).

emitters. In addition, as shown in Fig. 2d, the smaller effective Si–metal contact fraction in the Ag/LAF configuration further contributes to its higher ρ_c.

Additionally, NaCl was included as a test group for contact resistance because it was used in our previous work and is a pH-neutral salt. In that study, Ag/Al TOPCon solar cells were found to degrade faster than Ag/LAF TOPCon solar cells under NaCl exposure [12,15]. Interestingly, although both NaCl and $NaNO_3$ are neutral salts, NaCl induced a much stronger increase in ρ_c. After NaCl treatment, ρ_c rose to approximately 24.2 mΩ·cm^2 for Ag/Al contacts and 17.1 mΩ·cm^2 for Ag/LAF contacts. These values are substantially higher than those obtained after $NaNO_3$ treatment, which were around 3.3 mΩ·cm^2 for Ag/Al and 2.2 mΩ·cm^2 for Ag/LAF. Both contact types, therefore, exhibited more pronounced degradation under NaCl exposure. Notably, Ag/LAF contacts showed no evident degradation after $NaNO_3$ treatment, whereas $NaNO_3$ was sufficient to trigger degradation in Ag/Al contacts. For alkaline salt treatment with NaHCO3, the contact resistivity of Ag/Al increased from 0.49 to 0.63 mΩ·cm^2, whereas that of Ag/LAF increased from 2.6 to 4.4 mΩ·cm^2. This trend indicates that Ag/LAF contacts are more vulnerable under alkaline conditions.

As the pH of the nitrate solutions decreased from $NaNO_3$ to $AgNO_3$, $Zn(NO_3)_2$, and $Al(NO_3)_3$, an increasing trend in the ρ_c was observed for both contact types. For the Ag/Al contacts, the average ρ_c values increased to approximately 3.3, 10.3, 11.6, and 148.0 mΩ·cm^2, respectively. For the Ag/LAF contacts, ρ_c rose to about 2.2, 3.9, 12.5, and 221.4 mΩ·cm^2. It should be noted that when ρ_c exceeds ~200 mΩ·cm^2, reliable extraction becomes difficult at certain measurement locations due to both the extremely poor electrical contact conditions and the practical resolution limits of the TLM measurement setup. These points therefore indicate very high contact resistivity, at which efficient current transport across the metal–silicon interface is severely impeded. For samples treated with $Al(NO_3)_3$, the actual contact resistivity is therefore expected to be even higher than the extractable values. These results demonstrate a strong dependence of contact degradation on solution pH, with increasingly acidic environments causing progressively more severe deterioration of the metal–silicon interface. Notably, the Ag/LAF contacts exhibited a higher sensitivity to decreasing pH, consistent with the larger increases in series resistance and the more pronounced reductions in FF and PCE shown in Fig. 3. In contrast, although the Ag/Al contacts were comparatively less sensitive to acidity, they remained vulnerable to ionic contamination because of aluminium self-oxidation, with even nominally neutral or weakly acidic salts readily triggering contact degradation, as previously reported [12].

To further identify the degradation roots, FIB-SEM cross-sectional images were obtained, as shown in Fig. 4a and b, with the corresponding EDS elemental mappings presented in Figs. S3 and S4. In the control samples that did not undergo accelerated testing, neither the Ag/Al nor the Ag/LAF contacts exhibited any evident corrosion features. Based on the EDS results, the main differences between the Ag/Al and Ag/LAF contacts were associated with the amounts of Al and glass frit regions, as indicated by PbO, the major component of the glass frit. The Ag/LAF contacts contained a lower fraction of glass frit, and no pronounced Al related compounds were detected within the contact. In addition, the dominant functional contacts in the Ag/LAF configuration were located at the tops of the silicon pyramids. These microstructural features enable effective electrical contact formation in these TOPCon solar cells, respectively.

Under alkaline conditions, slight corrosion was observed in the Ag/Al contacts treated with $NaHCO_3$, particularly in regions where Al and glass frit were intermixed. In our previous work, $NaHCO_3$ was shown to cause extensive oxidation in these regions when the damp heat exposure time was sufficiently extended [12]. In addition, the glass frit interfacial layer of the Ag/LAF contacts was also affected by $NaHCO_3$ and exhibited clear corrosion features. This behaviour can be attributed to the alkaline environment generated by $NaHCO_3$, which releases OH^- ions that promote reactions with PbO in the glass frit, as described by Eq. (1) [51,52]. However, under the contaminant-limited ageing conditions applied in this work, the degradation response is also influenced by the effective availability of alkaline species and local chemical buffering effects at the contact interface. For the Ag/Al contacts, the corrosion features appear less pronounced in the present experiment. This may be attributed to the higher glass frit fraction in the Ag/Al paste compared with the Ag/LAF

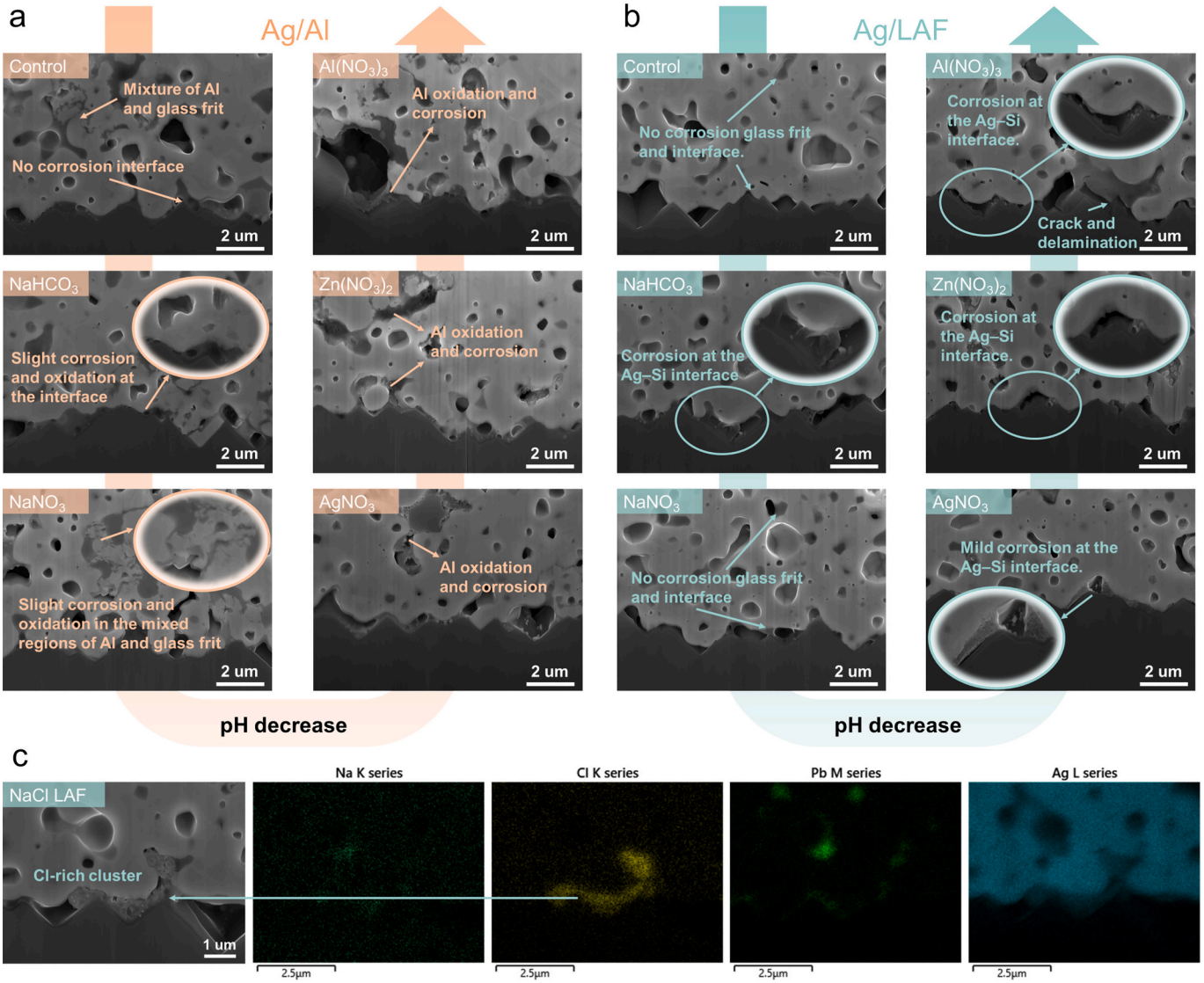

Fig. 4. FIB–SEM cross-sectional images of (a) Ag/Al and (b) Ag/LAF contacts after DH85 exposure to contaminants with different pH values, and (c) FIB–SEM cross-sectional with EDS elemental mapping of an Ag/LAF contact treated with NaCl.

formulation. In addition, Al present in the contact can react with hydroxyl species to form hydrated Al corrosion products, such as aluminium hydroxide or oxyhydroxide phases [53–55]. Under prolonged ageing conditions, these interfacial products might undergo gradual structural evolution or partial dehydration, potentially leading to the formation of relatively compact oxide-rich regions that can locally retard further degradation. This may be attributed to the higher glass frit fraction in the Ag/Al paste compared with the Ag/LAF formulation. Nevertheless, corrosion is still expected to proceed gradually through continued glass frit degradation in other regions. Under the 24-h exposure used in this study, these effects were therefore not clearly visible in the cross-sectional images.

$$PbO_{(s)} + OH^{-}{}_{(aq)} + H_2O_{(l)} \rightarrow \left[Pb(OH)_3^{-}\right]_{(aq)} \quad (1)$$

For $NaNO_3$, which represents a near-neutral chemical environment, slight corrosion features were observed at the Al–glass frit regions of the Ag—Si interface in the selected cross-sectional image. In contrast, no comparable fingerprints were detected in the Ag/LAF contacts. This disparity can be attributed to the presence and electrochemical role of Al in the Ag/Al contacts. As shown in Fig. 2c, Al plays a critical role in contact formation by penetrating the Si surface and forming local Al spikes. From an electrochemical perspective, metallic Al is significantly more active than Ag and can act as the anodic component in an Al—Ag galvanic couple. Consequently, Al is more susceptible to electron loss and preferential oxidation, even under near-neutral conditions. Under damp-heat conditions, the presence of $NaNO_3$ could further facilitate interfacial electrochemical reactions, thereby accelerating localized Al oxidation and corrosion at the metal–glass–Si interface. This behaviour is consistent with our previous observations, although the reaction kinetics are expected to depend on the specific anionic species present in the contaminants [12].

In contrast, the Ag/LAF contacts contain no Al and do not rely on Al-spike contact formation. Electrical conduction in these contacts is primarily enabled by localized Ag—Si alloying and AgNPs embedded within the glass frit. Moreover, both Na^+ and NO_3^- are chemically benign toward the Ag—Si interface and the SiN_x layer, likely providing no thermodynamic or electrochemical driving force to initiate interfacial corrosion or oxidation. As a result, no evident degradation of the Ag/LAF contacts could be observed after $NaNO_3$ exposure under DH85 conditions.

For $AgNO_3$, $Zn(NO_3)_2$, and $Al(NO_3)_3$ treatments, the corrosion features at the contacts were much more pronounced. This is primarily because these nitrate salts generate solutions with pH values below 7,

and the acidic environment can drive reactions with PbO (as shown in Eq. (2)) and other oxide components in the glass frit, leading to the formation of metal-containing salts [14,23]. Such corrosion fingerprints were observed in both Ag/Al and Ag/LAF contacts, and the extent of glass frit degradation scaled with the acidity of the solution.

$$PbO_{(s)} + 2H^{+}{}_{(aq)} \rightarrow Pb^{2+}{}_{(aq)} + H_2O_{(l)} \quad (2)$$

For the Ag/Al contacts, aluminium oxidation provided an additional degradation pathway. Under acidic conditions, NO_3^- can undergo reduction in this class of acidic nitrate solutions, such as $AgNO_3$, $Zn(NO_3)_2$, and $Al(NO_3)_3$. During this process, a fraction of NO_3^- can be reduced to gaseous by-products such as NO, N_2O, and N_2, which facilitates electron transfer and further promotes Al oxidation [35,36]. This mechanism has a much weaker impact on Ag/LAF contacts. In contrast, for Ag/Al contacts, where Al spikes are the dominant current-carrying pathways, contact degradation can be significantly accelerated.

Compared with other artificial ageing approaches, this degradation route is more physically relevant, because modules deployed in natural environments are inevitably exposed to oxygen and moisture, which can oxidise metal contacts over sufficiently long timescales [56–58]. Nitrate species effectively accelerate these intrinsically slow oxidation processes, thereby providing a closer approximation to realistic field-driven degradation.

The presence of metal cations further promoted Al self-oxidation, resulting in a faster degradation rate for Ag/Al contacts compared with Ag/LAF contacts when the pH was in the range of 5–6, as in the cases of $AgNO_3$ and $Zn(NO_3)_2$. In addition, chemical evolution of PbO-containing glass-frit phases under ionic ageing may lead to local weakening or discontinuity of the interfacial glass layer, thereby modifying transport pathways for moisture and dissolved species [59,60]. Such changes can increase the electrochemical accessibility of underlying Al-containing regions and promote localized corrosion processes. Consequently, the corrosion severity of Ag/LAF contacts could be primarily governed by the solution pH, whereas the degradation fingerprints of Ag/Al contacts were influenced by both pH-driven glass-frit corrosion and aluminium oxidation.

Additionally, we also used NaCl which is also a neutral salt, but it still resulted in significant contact degradation both on Ag/Al and Ag/LAF contacts. We have systematically investigated the Ag/Al contact failure caused by NaCl in previous work [12,15]. The fast degradation was due to the high penetration rate of Cl and Cl could easily accelerate the Al oxidation and corrosion [12,61–64]. However, differently we also noticed that NaCl had severe negative impact on Ag/LAF contact as well. Hence, we extracted a cross-sectional image and corresponding EDS as shown in Fig. 4c. The analysis indicates a localized enrichment of chlorine signals at the Ag/Si contact interface, accompanied by partial spatial co-localisation with Ag, suggesting the presence of corrosion-related interfacial species. This observation is consistent with our previous observations in low-temperature Ag paste in silicon heterojunction solar cells [29]. The AgNPs at the contact interface are highly reactive and could undergo chloride-induced dissolution–complexation reactions under humid conditions [65–68]. Cl^- ions readily interact with Ag and promote the formation of AgCl species, as described in Eq. (3).

$$Ag_{(s)} + Cl^{-}{}_{(aq)} \leftrightarrow AgCl_{(aq)} + e^- \quad (3)$$

Furthermore, AgCl can further complex with Cl^- ions to form soluble Ag—Cl complexes, such as $AgCl_2^-$, $AgCl_3^{2-}$, and $AgCl_4^{3-}$, under damp-heat conditions, as shown in Eq. (4) [69].

$$AgCl_{(s)} + (n-1)Cl^{-}{}_{(aq)} \leftrightarrow AgCl_n^{1-n} \quad (4)$$

These reactions could facilitate the dissolution and redistribution of AgNPs at the Ag/Si interface, which can disrupt the effective conductive routine and accelerate the degradation of the metallization contact. After the completion of the ageing process, the chemical equilibrium may shift and Ag can reprecipitate. However, the redeposited Ag is no longer in the original contact structure [69–71]. We could observe Ag and Cl EDS signals highly overlapped in certain regions as shown in Fig. 4c. Instead, it forms irregular or poorly connected Ag phases due to strong complexation with chloride species. As a result, the electrical conductivity of the contact deteriorates, leading to an increase in the R_s of the solar cell.

To further verify this mechanism, additional chloride salts were systematically investigated. The corresponding electrical performance results are presented in Table S2, while the degradation behaviour of Ag/LAF contacts is shown in Fig. S5. Similar degradation trends were consistently observed, providing further evidence that Cl^- ions can specifically interact with AgNPs and play a critical role in the metallization degradation process.

Notably, in NaCl-based cell-level tests, the detrimental impact of Cl^- on AgNPs stability appeared comparatively less pronounced. In contrast, significantly greater performance degradation was observed at equivalent chloride-ion concentrations in solutions containing potassium chloride (KCl), magnesium chloride ($MgCl_2$), calcium chloride ($CaCl_2$), and ammonium chloride (NH_4Cl). This variation is likely associated with cation-dependent ionic interactions and their influence on interfacial electrochemical reactions, including differences in ionic hydration behaviour, transport kinetics, and local electrochemical potential distribution [72]. In addition, distinct hydrolysis characteristics of multivalent or weakly acidic cations may induce variations in local interfacial acidity, thereby further accelerating Ag dissolution–complexation reactions and contact corrosion.

In contrast, NO_3^- are negatively charged oxyanions with oxidizing nature. However, unlike chloride ions, nitrate has little tendency to form stable coordination complexes with Ag under the tested conditions. Therefore, $NaNO_3$ mainly acts as an ionic electrolyte that influences the solution pH and ionic strength, while its direct involvement in metallization corrosion reactions is limited. Consequently, the degradation induced by $NaNO_3$ is significantly weaker compared with that caused by NaCl.

Further tests across different chloride systems consistently revealed pronounced degradation in Ag/LAF contacts, highlighting the intrinsic vulnerability of AgNPs-dominated conduction networks. In Ag/LAF metallization schemes, AgNPs contribute not only to Ag—Si contact formation at pyramid tips but also to the overall current transport network, making these contacts particularly susceptible to chloride-induced corrosion. Although NaCl-based accelerated tests can already differentiate the degradation behaviour of TOPCon cells employing Ag/Al and Ag/LAF contacts, this simplified mechanism still does not fully capture the complex degradation pathways occurring in practical TOPCon modules.

Systematic testing across multiple chloride salts consistently revealed pronounced degradation in Ag/LAF contacts, highlighting the intrinsic vulnerability of AgNPs-dominated conduction networks. In Ag/LAF metallization schemes, AgNPs contribute not only to Ag—Si contact formation at pyramid tips but also to the overall current transport network, rendering these contacts particularly susceptible to Cl-induced corrosion. Although NaCl-based accelerated tests can effectively differentiate the degradation behaviour of TOPCon cells employing conventional Ag/Al and Ag/LAF contacts, such simplified conditions mainly isolate chloride-driven reactions. Therefore, they cannot fully capture the coupled physicochemical degradation pathways that occur in practical TOPCon module environments [7,15]. By contrast, under relatively mild acidic conditions, NO_3^- does not react with AgNPs. Moreover, nitrates are universal in the environment and in module glass. Therefore, using nitrate-based solutions may provide a more realistic and physically meaningful approach for accelerated reliability testing.

3.3. Validation of consistency between cell-level accelerated ageing and module-level degradation in TOPCon devices

Based on the work reported by Park et al., EVA-based encapsulant

materials exhibit a mildly acidic environment with a pH close to 5 [31]. Consistent with this, and informed by our previous experiments, the Zn $(NO_3)_2$ exposure duration was extended from 24 h to 60 h (pH ≈ 5.1) to evaluate front-side contact degradation in TOPCon solar cells under prolonged stress. The corresponding relative changes in I—V parameters are summarized in Fig. 5a and Table S3.

Under these conditions, Ag/Al TOPCon solar cells exhibited an approximately 10.0% relative PCE loss, primarily driven by a 9.5% relative reduction in FF due to an ~1500% increase in R_s. In contrast, solar cells with Ag/LAF contacts showed a smaller PCE degradation of $4.2\%_{rel}$, again dominated by an FF decrease ($3.8\%_{rel}$). In both cases, changes in J_{sc} (or I_{sc}) and V_{oc} contributed only marginally to the overall PCE loss. In addition, the relative variations in PL and R_s mapping, shown in Fig. 5c and d, further indicate that the dominant degradation fingerprints are localized in the solar cells' metallisation regions.

At the module level, double-glass EVA-encapsulated TOPCon modules exhibited relative PCE losses of ~6.2% for Ag/Al and ~ 3.6% for Ag/LAF, respectively, as shown in Fig. 5a and Table S4. The corresponding EL images in Fig. 5b show that the dominant failure sites are also concentrated in the metallisation regions, confirming that metallisation degradation is the primary source of the performance differences between these two module types. Although a slight decrease in I_{sc} was also observed, this is likely attributable to encapsulant ageing under DH85 conditions. The dominant contributor to the PCE divergence remains the difference in FF loss, which is closely linked to contact degradation.

While direct quantitative comparability between cell-level accelerated ageing and module-level degradation cannot be established within the scope of this study, a qualitatively similar FF-related degradation tendency between the two metallisation methods was observed at both the cell and module levels. This observation supports the practical relevance of the proposed front-side metallisation assessment approach for TOPCon devices, as it enables targeted evaluation of contact stability under chemically moderated, EVA-relevant acidic conditions. In contrast, module-level performance loss may be additionally influenced by encapsulation-driven ageing effects, which can contribute to enhanced I_{sc}/J_{sc} degradation and obscure intrinsic contact reliability behaviour. Therefore, the present method provides a more controlled framework for mechanistic comparison of emerging metallisation architectures compared with conventional soaking- or mist-based tests, which often induce overly aggressive or poorly differentiated degradation pathways.

These findings further highlight the limitations of CH_3COOH immersion testing, since complete immersion introduces highly aggressive liquid-phase conditions with abundant electrolyte availability, which can promote rapid corrosion reactions that may not be representative of the chemically moderated ageing environments encountered in encapsulated modules over long-term operation [13,14]. The discrepancy between CH_3COOH soaking results and module-level degradation highlights the need for test methodologies that provide more controlled and chemically moderated ageing conditions, enabling clearer differentiation of metallisation reliability behaviour.

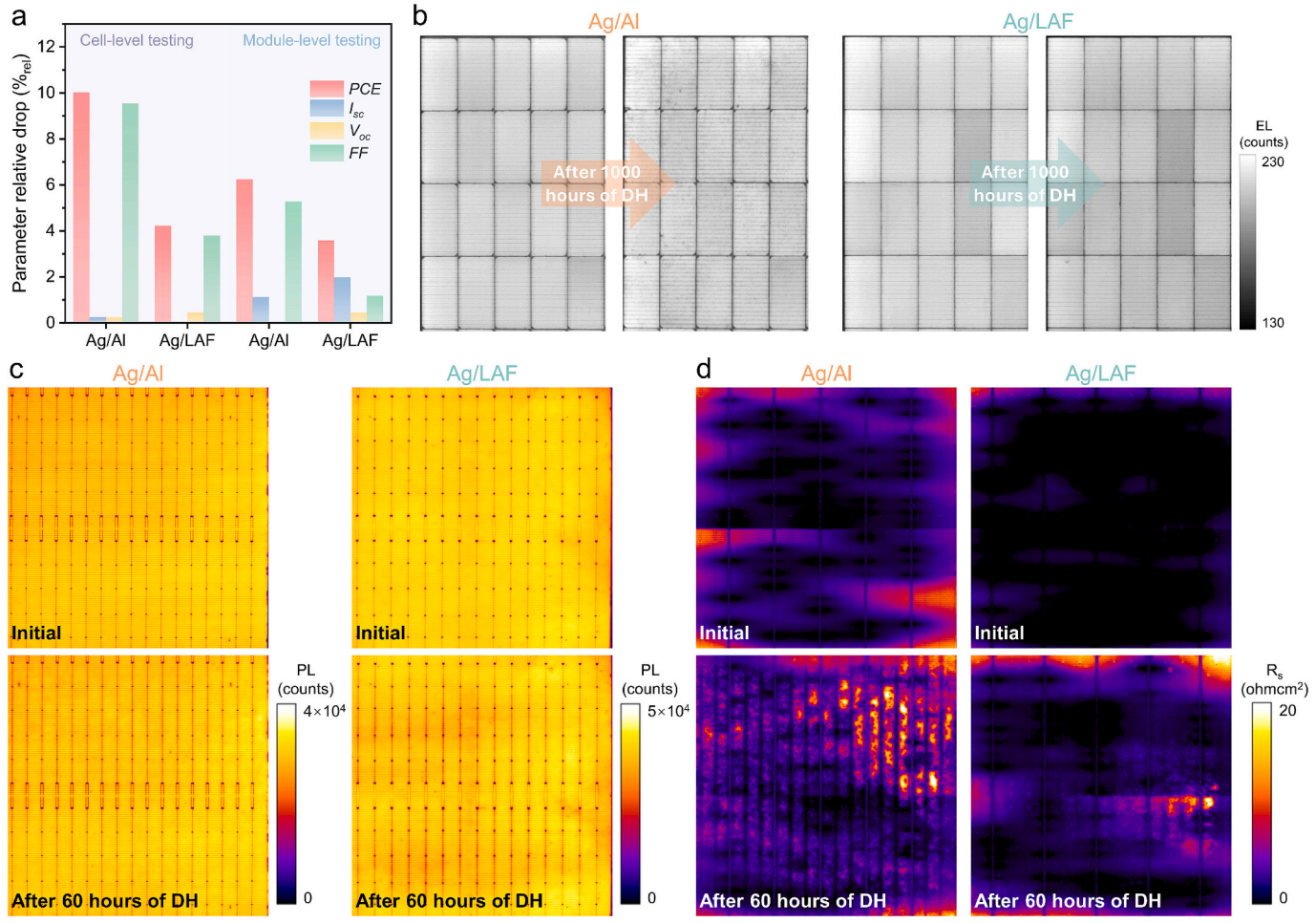

Fig. 5. (a) Relative I—V parameter variations of TOPCon solar cells after 60 h accelerated DH85 testing following $Zn(NO_3)_2$ treatment, and relative I—V parameter variations of Ag/Al and Ag/LAF modules after 1000 h of DH85 testing; (b) EL images of B-G TOPCon modules encapsulated with EVA before and after 1000 h of DH85 testing; (c) PL and (d) R_s images of Ag/Al and Ag/LAF TOPCon solar cells before and after 60 h accelerated DH85 testing following $Zn(NO_3)_2$ treatment.

The results further highlight the importance of carefully selecting induced contaminants in accelerated testing. Although chloride ions can trigger distinct degradation pathways in AgNPs-based contacts, significant Cl accumulation inside modules is unlikely outside Cl-rich environments such as offshore, saline, or industrial regions. Consequently, the routine use of Cl-related salts in accelerated tests may introduce artificial degradation mechanisms that do not occur under typical field conditions, thereby potentially misleading metallisation design or process optimisation.

In addition, other ionic species, such as $NaHCO_3$, may fail to accurately represent module-level degradation behaviour. The alkaline environment generated by such salts can activate alternative failure mechanisms that are not relevant to the chemical conditions experienced inside encapsulated modules, further limiting the physical relevance of these accelerated test conditions.

From a methodological perspective, the use of chemically relevant species whose elemental composition and ionic forms already exist within solar cell and module environments offers a pathway toward more physically grounded accelerated reliability testing. This strategy minimises the risk of introducing foreign degradation drivers and enhances the predictive value of short-term tests for long-term field performance. Overall, the proposed framework provides a foundation for developing next-generation accelerated ageing protocols that balance test severity with physical realism, thereby supporting more reliable metallisation engineering for advanced TOPCon technologies.

4. Conclusions

This study shows that conventional solution-based soaking tests, such as CH_3COOH immersion, can impose chemically unrealistic and non-selective stress conditions on TOPCon solar cells and therefore are not representative of module-level reliability. In particular, such tests tend to overemphasise contact degradation in Ag/LAF solar cells and do not reproduce the degradation trends observed under damp-heat conditions in encapsulated modules, highlighting their restricted predictive relevance.

To address this issue, a chemically relevant, single-side spray-based accelerated testing approach was developed to enable selective evaluation of front-side contact stability under controlled pH conditions. Using nitrate-based salts with systematically varied acidity, a clear pH-dependent degradation trend was observed for both Ag/Al and Ag/LAF metallisation schemes. With increasing acidity, both contact types showed increases in contact resistivity and series resistance, resulting in dominant FF and PCE losses. Under weakly acidic nitrate conditions [$Zn(NO_3)_2$, pH $\approx$ 5, at 25 °C], which are relevant to EVA-associated acidic environments, degradation at the cell level was dominated by contact resistivity increases and FF-related performance losses.

From an engineering perspective, the proposed methodology provides a controlled framework for comparative assessment of emerging metallisation architectures. By selecting chemically moderated ionic species and applying spatially selective stress, the approach improves the interpretability of degradation fingerprints obtained from accelerated cell-level testing without inducing excessively aggressive ageing conditions. While quantitative correlation with long-term module degradation remains beyond the scope of this work, the framework offers a useful basis for mechanistic screening and early-stage reliability differentiation of advanced solar cell metallisation designs.

Beyond TOPCon technology, the proposed chemically relevant cell-level ageing framework may also be extendable to other advanced silicon and hybrid photovoltaic architectures, including silicon heterojunction, back-contact, and perovskite-silicon tandem solar cells, where metallisation stability under mildly acidic moisture ingress is a critical reliability bottleneck.

CRediT authorship contribution statement

Xinyuan Wu: Writing – review & editing, Writing – original draft, Visualization, Methodology, Investigation, Formal analysis, Data curation, Conceptualization. **Wei Wu:** Investigation, Formal analysis, Data curation. **Weiguang Yang:** Investigation, Funding acquisition, Formal analysis. **Yan Zhang:** Methodology, Investigation, Formal analysis. **Jiexi Fu:** Investigation, Formal analysis, Data curation. **Xutao Wang:** Investigation, Formal analysis, Data curation. **Jing Yuan:** Investigation, Formal analysis. **Jianjun Nie:** Investigation, Formal analysis. **Zhencong Qiao:** Investigation, Formal analysis. **Chao An:** Resources, Investigation, Formal analysis. **Feng Li:** Investigation, Formal analysis. **Lin Lv:** Investigation, Formal analysis. **Baochen Liao:** Writing – review & editing, Methodology, Investigation, Formal analysis. **Bram Hoex:** Writing – review & editing, Supervision, Resources, Project administration, Methodology, Funding acquisition, Formal analysis, Data curation.

Declaration of competing interest

The authors declare that they have no known competing financial interests or personal relationships that could have appeared to influence the work reported in this paper.

Acknowledgements

The authors from Jolywood (Taizhou) gratefully acknowledge financial support from the National Key Research and Development Program of China (Grant No. 2022YFB4200902). This work is supported by the Australian Centre for Advanced Photovoltaics (ACAP) and received funding from the Australian Renewable Energy Agency (ARENA) as well as the Australian Government's Trailblazer for Recycling & Clean Energy program, led by UNSW & the University of Newcastle. However, the Australian Government does not accept responsibility for the views, information, or advice expressed in this research. The authors would like to acknowledge the Electron Microscope Unit at The University of New South Wales (UNSW), specifically Dr. Charlie Kong and Dr. Yin Yao, for their scientific and technical assistance and access to the facilities of the Australian Microscopy & Microanalysis Research Facility. The authors also express their gratitude for the support provided by the entire team at the Solar Industrial Research Facility (SIRF) at UNSW. During the preparation of this work, the authors used GPT-5.2 in order to improve the readability and language of the work. After using this tool, the authors reviewed and edited the content as needed and take full responsibility for the content of the publication.

Appendix A. Supplementary data

Supplementary data to this article can be found online at https://doi.org/10.1016/j.cej.2026.175634.

Data availability

Data will be made available on request.

References

[1] D.K. Ghosh, et al., Fundamentals, present status and future perspective of TOPCon solar cells: a comprehensive review, Surf. Interfaces 30 (2022) 101917.
[2] M. Fischer, M. Woodhouse, P. Baliozian, J. Trube, International Technology Roadmap for Photovoltaic (ITRPV) 2024 Results, VDMA, 2025.
[3] B. Kafle, B.S. Goraya, S. Mack, F. Feldmann, S. Nold, J. Rentsch, TOPCon – Technology options for cost efficient industrial manufacturing, Sol. Energy Mater. Sol. Cells 227 (2021) 111100.
[4] PV Bill of Material Market Report, InfoLink, 2026.
[5] M.M. Kristoff, Viability Assessment of New Domestic Solar Module Manufacturing Units–Can India Compete Against China in PV Production?, 2021.

[6] P. Hacke, S. Spataru, B. Habersberger, Y. Chen, Field-representative evaluation of PID-polarization in TOPCon PV modules by accelerated stress testing, Prog. Photovolt. Res. Appl. 32 (5) (2024) 346–355.
[7] X. Wu, et al., Is TOPCon ready for EVA? Insights from damp heat testing of glass-backsheet modules, Sol. Energy Mater. Sol. Cells 288 (2025) 113650.
[8] C. Sen, et al., Buyer aware: three new failure modes in TOPCon modules absent from PERC technology, Sol. Energy Mater. Sol. Cells 272 (2024) 112877.
[9] M.U. Khan, et al., UV-induced degradation in TOPCon solar cells: Hydrogen dynamics and impact of UV wavelength, Sol. Energy Mater. Sol. Cells 294 (2026) 113895.
[10] F.T. Thome, et al., UV-Induced Degradation of Industrial PERC, TOPCon, and HJT Solar Cells: The Next Big Reliability Challenge? Sol. RRL 8 (23) (2024) 2400628.
[11] P. Gebhardt, U. Kräling, E. Fokuhl, I. Hädrich, D. Philipp, Reliability of Commercial TOPCon PV Modules—An Extensive Comparative Study, Prog. Photovolt. Res. Appl. 33 (12) (2025) 1378–1386.
[12] X. Wu, et al., Unveiling the origin of metal contact failures in TOPCon solar cells through accelerated damp-heat testing, Sol. Energy Mater. Sol. Cells 278 (2024) 113188.
[13] Y. Chen Li, et al., Degradation mechanism of TOPCon solar cells in an ambient acid environment, ACS Appl. Mater. Interfaces 17 (7) (2025) 10776–10783.
[14] N. Iqbal, et al., Impact of acetic acid exposure on metal contact degradation of different crystalline silicon solar cell technologies, Sol. Energy Mater. Sol. Cells 250 (2023) 112089.
[15] X. Wu, et al., Enhancing the reliability of TOPCon technology by laser-enhanced contact firing, Sol. Energy Mater. Sol. Cells 271 (2024) 112846.
[16] Y. Ye, et al., Damp-heat stability investigation of glass-backsheet modules based on TOPCon solar cells, Sol. Energy Mater. Sol. Cells 292 (2025) 113764.
[17] Y. Zhou, D. Chen, Y. Ye, H. Yin, X. Niu, Damp-heat endurance investigation of PV modules based on n-type bifacial passivated contact cells, in: European Photovoltaic Solar Energy Conference and Exhibition 2023, 2023.
[18] Q. Wang, K. Guo, S. Gu, W. Huang, W. Wu, J. Ding, Investigation on effects of the laser-enhanced contact optimization process with ag paste in a boron emitter for n-TOPCon solar cell, Prog. Photovolt. Res. Appl. 33 (2) (2025) 294–308.
[19] X. Wang, et al., Higher-efficiency TOPCon solar cells in mass production enabled by laser-assisted firing: advanced loss analysis and near-term efficiency potential, Prog. Photovolt. Res. Appl. 33 (7) (2025) 771–781.
[20] O.K. Segbefia, A.G. Imenes, T.O. Sætre, Moisture ingress in photovoltaic modules: a review, Sol. Energy 224 (2021) 889–906.
[21] M. Tiefenthaler, G.M. Wallner, R. Pugstaller, Effect of global damp heat ageing on debonding of crosslinked EVA- and POE-glass laminates, Sol. Energy Mater. Sol. Cells 264 (2024) 112602.
[22] T. Semba, Correlation between the metallization corrosion and acetic acid in crystalline silicon photovoltaic module, Jpn. J. Appl. Phys. 59 (11) (2020) 114001.
[23] A. Kraft, et al., Investigation of acetic acid corrosion impact on printed solar cell contacts, IEEE J. Photovoltaics 5 (3) (2015) 736–743.
[24] C. Peike, et al., Origin of damp-heat induced cell degradation, Sol. Energy Mater. Sol. Cells 116 (2013) 49–54.
[25] M.D. Kempe, G.J. Jorgensen, K.M. Terwilliger, T.J. McMahon, C.E. Kennedy, T. T. Borek, Acetic acid production and glass transition concerns with ethylene-vinyl acetate used in photovoltaic devices, Sol. Energy Mater. Sol. Cells 91 (4) (2007) 315–329.
[26] X. Li, et al., Potential-free sodium-induced degradation of silicon heterojunction solar cells, in: Progress in Photovoltaics: Research and Applications, 2023.
[27] D. Adachi, T. Terashita, T. Uto, J.L. Hernández, K. Yamamoto, Effects of SiOx barrier layer prepared by plasma-enhanced chemical vapor deposition on improvement of long-term reliability and production cost for Cu-plated amorphous Si/crystalline Si heterojunction solar cells, Sol. Energy Mater. Sol. Cells 163 (2017) 204–209.
[28] H. Tong, et al., Mitigating contaminant-induced surface degradation in TOPCon solar cells: mechanisms, impacts, and mitigation, Sol. Energy Mater. Sol. Cells 286 (2025) 113558.
[29] X. Wu, et al., Unveiling the degradation mechanisms in silicon heterojunction solar cells under accelerated damp-heat testing, Sol. Energy Mater. Sol. Cells 282 (2025) 113325.
[30] Y. Luo, et al., Sodium-induced degradation of tungsten doped indium oxide film and HJT solar cells in damp-heat environment, Sol. Energy 296 (2025) 113578.
[31] G. Park, et al., The origin of the HJT silicon solar cell degradation induced by indium tin oxide corrosion, Prog. Photovolt. Res. Appl. (2025), https://doi.org/10.1002/pip.70051.
[32] J.L. Jackel, Glass waveguides made using low melting point nitrate mixtures, Appl. Opt. 27 (3) (1988) 472–475.
[33] L.G. van Uitert, W.H. Grodkiewicz, Nitrate glasses, Mater. Res. Bull. 6 (4) (1971) 283–291.
[34] E.P. Rao, K. Puttanna, Nitrates, agriculture and environment, Curr. Sci. 79 (9) (2000) 1163–1168.
[35] J.C. Fanning, The chemical reduction of nitrate in aqueous solution, Coord. Chem. Rev. 199 (1) (2000) 159–179.
[36] M. De Groot, M. Koper, The influence of nitrate concentration and acidity on the electrocatalytic reduction of nitrate on platinum, J. Electroanal. Chem. 562 (1) (2004) 81–94.
[37] H. Hassani, V.M. Sglavo, Effect of Na contamination on the chemical strengthening of soda-lime silicate float glass by ion-exchange in molten potassium nitrate, J. Non-Cryst. Solids 515 (2019) 143–148.
[38] F.M. Padilla, M. Gallardo, F. Manzano-Agugliaro, Global trends in nitrate leaching research in the 1960–2017 period, Sci. Total Environ. 643 (2018) 400–413.
[39] IEC TS 62782:2016, Photovoltaic (PV) Modules - Cyclic (dynamic) Mechanical Load Testing, I. E. Commission, 2016, 2016-03-09. [Online]. Available: https://webstore.iec.ch/publication/24310.
[40] D.N.R. Payne, C. Vargas, Z. Hameiri, S.R. Wenham, D.M. Bagnall, An advanced software suite for the processing and analysis of silicon luminescence images, Comput. Phys. Commun. 215 (2017) 223–234.
[41] S. Burgess, P. Pinard, AZtec wave–a new way to achieve combined EDS and WDS capability on SEM, Microsc. Microanal. 26 (S2) (2020) 114–115.
[42] G. Xing, W. Chen, Y. Liu, X. Du, Al-induced variation to Ag crystal orientation of Ag–Al pastes during metallization, Sol. Energy Mater. Sol. Cells 270 (2024) 112814.
[43] P. Zhu, Y. Liu, C. Cao, J. Tian, A. Zhang, D. Wang, Low recombination firing-through Al paste for N-type solar cell with boron emitter, Materials 14 (4) (2021) 765.
[44] P. Afzali, M. Yousefpour, E. Borhani, Effect of deformation-induced defects on the microstructure and pitting corrosion behavior of Al-Ag alloy, Int. J. Eng. 31 (12) (2018) 2092–2101.
[45] N. Wöhrle, E. Lohmüller, J. Greulich, S. Werner, S. Mack, Towards understanding the characteristics of Ag–Al spiking on boron-doped silicon for solar cells, Sol. Energy Mater. Sol. Cells 146 (2016) 72–79.
[46] E. Lohmüller, S. Werner, R. Hoenig, J. Greulich, F. Clement, Impact of boron doping profiles on the specific contact resistance of screen printed Ag–Al contacts on silicon, Sol. Energy Mater. Sol. Cells 142 (2015) 2–11.
[47] Y. Fan, et al., Investigation of the Ag–Si contact characteristics of boron emitters for n-tunnel oxide-passivated contact solar cells metallized by laser-assisted current injection treatment, Sol. RRL 8 (13) (2024).
[48] B. Feng, Y. Liu, W. Chen, G. Xing, X. Chen, X. Du, Differently shaped Ag crystallites and four current transport paths at sintered Ag/Si interface of crystalline silicon solar cells, Sol. Energy Mater. Sol. Cells 257 (2023) 112381.
[49] T. Oza, V. Oza, R. Thaker, The thermal decomposition of silver nitrite, J. Chem. Soc. (1955) 2457–2465.
[50] B.V. L'vov, A.V. Novichikhin, Mechanism of thermal decomposition of anhydrous metal nitrates, Spectrochim. Acta B At. Spectrosc. 50 (12) (1995) 1427–1448.
[51] J. Carr, N. Hampson, R. Taylor, The electrochemical behaviour of PbO2 in Alkali, Ber. Bunsenges. Phys. Chem. 74 (6) (1970) 557–561.
[52] A.A. Abdul Azim, K.M. El-Sobki, Corrosion and passivity of Pb in strongly alkaline solutions, Corros. Sci. 12 (3) (1972) 207–215.
[53] M. Paez, et al., Anodic oxidation of Al–Ag alloys, Corros. Sci. 44 (12) (2002) 2857–2863.
[54] C. Chang, et al., Aluminum oxidation in water, J. Electrochem. Soc. 125 (5) (1978) 787–792.
[55] L. Aleksandr, P. Alexander, B. Olga, K. Sergey, G. Irena, Synthesis of antimicrobial AlOOH–Ag composite nanostructures by water oxidation of bimetallic Al–Ag nanoparticles, RSC Adv. 8 (63) (2018) 36239–36244.
[56] A.A. Hasan, et al., A review on silicon photovoltaic module degradations and recent identification techniques, Sol. Energy 288 (2025) 113288.
[57] R. Meena, A. Pareek, R. Gupta, A comprehensive review on interfacial delamination in photovoltaic modules, Renew. Sust. Energ. Rev. 189 (2024) 113944.
[58] O.K. Segbefia, N. Akhtar, T.O. Sætre, Moisture induced degradation in field-aged multicrystalline silicon photovoltaic modules, Sol. Energy Mater. Sol. Cells 258 (2023) 112407.
[59] H. Li, X. Sun, J. Xing, Y. Yang, X. Yuan, H. Tong, Effect of glass frit composition on reliability of silver paste metallization in crystalline silicon solar cells, Mater. Res. Express 11 (5) (2024) 056303.
[60] Z. Guo, J. Liu, X. Zhou, Y. Sun, H. Yu, S. Ma, Characterizing glass frits for high efficiency crystalline silicon solar cells by etching experiments, Sol. Energy Mater. Sol. Cells 276 (2024) 113065.
[61] A. Gnedenkov, S. Sinebryukhov, D. Mashtalyar, I. Vyaliy, V. Egorkin, S. Gnedenkov, Corrosion of the welded aluminium alloy in 0.5 M NaCl solution. Part 1: specificity of development, Materials 11 (10) (2018) 2053.
[62] M. Jingling, W. Jiuba, L. Gengxin, X. Chunhua, The corrosion behaviour of Al–Zn–In–Mg–Ti alloy in NaCl solution, Corros. Sci. 52 (2) (2010) 534–539.
[63] Q. Zhang, Z. Zhang, On the electrochemical dealloying of Al-based alloys in a NaCl aqueous solution, Phys. Chem. Chem. Phys. 12 (7) (2010) 1453–1472.
[64] Y. Li, M. Spiegel, S. Shimada, Corrosion behaviour of various model alloys with NaCl–KCl coating, Mater. Chem. Phys. 93 (1) (2005) 217–223.
[65] L. Li, Y.-J. Zhu, High chemical reactivity of silver nanoparticles toward hydrochloric acid, J. Colloid Interface Sci. 303 (2) (2006) 415–418.
[66] R. Prucek, et al., Re-crystallization of silver nanoparticles in a highly concentrated NaCl environment—a new substrate for surface enhanced IR-visible Raman spectroscopy, Cryst. Eng. Comm. 13 (7) (2011) 2242.
[67] K.A. Huynh, K.L. Chen, Aggregation kinetics of citrate and polyvinylpyrrolidone coated silver nanoparticles in monovalent and divalent electrolyte solutions, Environ. Sci. Technol. 45 (13) (2011) 5564–5571.
[68] J. Yang, Q. Zhang, J.Y. Lee, H.-P. Too, Dissolution–recrystallization mechanism for the conversion of silver nanospheres to triangular nanoplates, J. Colloid Interface Sci. 308 (1) (2007) 157–161.
[69] J.J. Fritz, Thermodynamic properties of chloro-complexes of silver chloride in aqueous solution, J. Solut. Chem. 14 (12) (1985) 865–879.

[70] X. Jin, J. Lu, P. Liu, H. Tong, The electrochemical formation and reduction of a thick AgCl deposition layer on a silver substrate, J. Electroanal. Chem. 542 (2003) 85–96.
[71] T.E. Graedel, Corrosion mechanisms for silver exposed to the atmosphere, J. Electrochem. Soc. 139 (7) (1992) 1963.
[72] H. Ha, J. Payer, The effect of silver chloride formation on the kinetics of silver dissolution in chloride solution, Electrochim. Acta 56 (7) (2011) 2781–2791.